Journal Name

ARTICLE

Electronic structure of the para-dinitrobenzene radical anion: A combined 2D photoelectron imaging and computational study

Received 00th January 20xx,
Accepted 00th January 20xx

DOI: 10.1039/x0xx00000x

www.rsc.org/

Cate S. Anstöter,[a,c] Thomas E. Gartmann,[b] Laurence H. Stanley,[a] Anastasia V. Bochenkova,*[c] and Jan R. R. Verlet *[a]

The para-dinitrobenzene radical anion has been studied by 2D photoelectron imaging within the energy range of 2.5 eV above the detachment threshold. Supporting electronic structure calculations at the XMCQDPT2 level of the excited states and resonances are presented. The direct photodetachment channel has been observed and modelled, and yields an electron affinity of 1.99±0.01 eV. In addition to the direct channel, evidence of resonances is observed. These resonances, which are symmetry allowed for photoexcitation from the ground state and of Feshbach types with respect to the open continuum, result in fast internal conversion to bound electronic states, followed by statistical electron emission observed at very low kinetic energies as well as dissociation of the nitrite anion. The latter is seen in the photoelectron spectra, which can be modelled as a combination of direct detachment from the para-dinitrobenzene and nitrite anions. An additional dimension has been offered by the 2D photoelectron angular distribution that is particularly sensitive to a mechanism of electron detachment, allowing us to confidently interpret the production of the nitrite anion photofragment.

Introduction

Electron driven chemistry underpins a wide range of chemical processes and technologies.[1–5] From a fundamental perspective, the primary step is the attachment of an electron to a neutral molecule mediated by electronic states of the anion. As these states lie above the neutral adiabatic energy, the electronic states are resonances and electron loss is always an open channel. It is the dynamics of these resonances that determine the fate of the reaction, be it electron loss, dissociative electron attachment, or parent anion formation. A particularly elegant method for probing signatures of these dynamics is 2D electron energy loss spectroscopy, in which the electron energy loss spectra were measured as a function of incoming electron kinetic energy (eKE).[6–9] We have recently developed an optical variant in which the photoelectron (PE) images are acquired as a function of photon energy ($h\nu$).[10–12] Here, we present such a 2D PE imaging study and employ high-level electronic structure calculations to unravel the information-rich spectra of the para-dinitrobenzene radical anion ($pDNB^-$).

Radical anions of dinitrobenzenes are fascinating because they are some of the simplest organic mixed valence systems. Meta- and para-dinitrobenzene (mDNB and pDNB) illustrate two examples of different classes of organic mixed-valence systems, as defined by the Robin-Day classification,[13] which is based on the electronic interaction between two redox sites within a molecule (the two nitro-groups in DNBs). For pDNB, there is strong electronic coupling between the two sites and the charge is entirely delocalised (class III). In contrast, mDNB exhibits weak electronic coupling between the two redox sites and the excess charge is localised on one of the NO_2 groups. Mixed-valence systems and intervalence charge-transfer transitions are extensively used in chemistry.[14,15] Most of this work and our understanding of mixed-valence systems have come from solution phase work, where interactions with the solvent affect the electronic structure. To explore the intrinsic electronic structure of mixed-valence systems, studies on the isolated molecules are desirable. Here, we study the class III strongly coupled $pDNB^-$, for which most of the excited states are not bound. The use of PE spectroscopy in combination with *ab initio* calculations allows us to gain insight into the intrinsic electronic structure of $pDNB^-$ and the decay mechanisms of the resonances.

The most commonly used computational method for exploring the electronic structure and properties of organic mixed-valence systems is density functional theory (DFT). DFT is often hailed as a compromise between reasonable accuracy and computational cost, however, for mixed-valence systems, specific care must be taken when choosing the functional. For hybrid functionals with too little Hartree-Fock (HF) exchange, charge delocalization is consistently overestimated; whereas too much HF exchange over localizes the charge.[16,17] A correct description of the Robin-Day classification can be obtained using these DFT methods, but it is not always due to a correct treatment of the intrinsic chemical physics of the molecule.

[a] Department of Chemistry, Durham University, Durham DH1 3LE, United Kingdom, Email: j.r.r.verlet@durham.ac.uk
[b] Lab. Für Physikal. Chemie, ETH Zürich, Vladimir-Prelog-Weg 2, 8093 Zürich, Switzerland
[c] Department of Chemistry, Lomonosov Moscow State University, 119991 Moscow, Russia, Email: bochenkova@phys.chem.msu.ru
Electronic Supplementary Information (ESI) available: the PE and β_2 spectra and CASSCF and XMCQDPT2 schemes; See DOI: 10.1039/x0xx00000x

While a thorough study by Sutton *et al*. showcases a reliable DFT methodology,[18] here we use extended multi-configurational quasi-degenerate perturbation theory (XMCQDPT2)[19] as a rigorous method that avoids any potential errors.

The study of pDNB$^-$ here is also motivated by our longer-term goal of probing intervalence charge-transfer processes in real-time using time-resolved PE spectroscopy. This requires knowledge of the electronic "structure" of the continuum, because the probe energy may access resonances that alter the observed PE spectra and lead to incorrect interpretations. This is likely to be a problem for pDNB$^-$ because of its high density of states.

Finally, while developing an understanding of the electronic structure of pDNB$^-$ builds on an understanding of mixed-valence systems, aromatic nitro-compounds also have important industrial uses and form the basis of many explosives.[20,21] Electron impact ionisation coupled to mass-spectrometry is a common analytical method used to detect trace amounts of such explosives. Although cations are detected because 70 eV electron are used in the ionisation step, low energy electrons may provide more distinctive fragmentation patterns when probing negatively-charged species.[22] To understand the possible dissociative electron attachment channels, several electron attachment studies have been performed on aromatic nitro-compounds.[23,24] Our work here complements these studies and the 2D PE spectra and 2D photoelectron angular distributions (PADs) combined with the computational work provides new insight into the resonances that lead to dissociative electron attachment in pDNB.

Methodology

Experimental

The experimental details are provided elsewhere and only a summary is given here.[25] Anions were produced by electrospray ionisation of a ~1 mM solution of pDNB dissolved in methanol. The DNB anions were introduced into vacuum by a capillary tube and guided through a series of differentially pumped regions by a series of ring-electrode ion guides that terminated in a trap.[26] From the trap, anions were pulsed into a collinear Wiley-McLaren time-of-flight mass spectrometer towards a velocity map imaging (VMI) assembly. Mass-selected ion packets were then intersected with light pulses generated by a tunable nanosecond laser pulse generated from a Nd:YAG pumped optical parametric oscillator and photodetached electrons were imaged using the VMI assembly. The Polar Onion Peeling algorithm was used to extract both the PE spectrum and PE PADs from raw images.[27] The PE spectra were calibrated using the known atomic spectrum of I$^-$ and have experimental resolution of ~5%.

Computational

All initial ground state calculations of pDNB anion and neutral species were carried out using the QChem 5.0 package.[28] Geometries were obtained at the MP2/aug-cc-pVDZ level of theory and verified to be minimum energy structures by vibrational analysis. Both the anion and neutral have D_{2h} symmetry, although all calculations were not restricted to this symmetry. The ground state of the radical anion is a $^2B_{2u}$ state while the neutral has a ^1A_g ground state.

The vertical excitation energies (VEEs) were calculated with extended multi-configurational quasi-degenerate perturbation theory (XMQCDPT2)[19] using the Firefly computational package.[29] This method was shown to perform exceptionally well for excited state calculations in the presence of a continuum and previously provided valuable insight into the dynamics and structure of anion resonances.[30,31] The excited states of pDNB$^-$ were calculated using an active space of 12 valence π-orbitals and 15 electrons. In order to include all states within our experimental range, we employed the XMCQDPT2[11]/SA(9)-CASSCF(15,12) method with a reference space spanned by 11 CASCI wavefunctions, which were obtained through complete active space self-consistent field (CASSCF) calculations using a state averaging procedure (SA). A DFT/PBE0-based one-electron Fock-type matrix was used to obtain energies of all CASSCF semi-canonical orbitals used in perturbation theory. For all calculations, the (aug)-cc-pVTZ basis set was used, where the augmented function was only affixed to the oxygen atoms of the nitro-groups. To calculate the vertical detachment energy (VDE), an extremely diffuse p-function was added to one of the carbon atoms of the ring. A single π* orbital of this highly diffuse shell was included in the active space and was used to mimic an electron-detachment process. The anion ground and bound excited states as well as the electron detached state were included in a state-averaging procedure for calculating the VDE at the XMCQDPT2[9]/SA(4)-CASSCF(15,13) level. Additionally, we performed the n-π* VEE calculations using the XMCQDPT2[11]/SA(11)-CASSCF(19,14) method by adding two n-orbitals to the π valence active space.

The PE spectra of the pDNB and nitrite anions were simulated at 300 K by direct evaluation of Franck-Condon integrals within the double harmonic parallel-mode approximation. Stick spectra were convoluted with Gaussian functions with a half width at half maximum of 12 meV. For this type of calculations, vibrational analysis and geometry optimization for the closed-shell species, pDNB and NO_2^-, were performed using MP2/(aug)-cc-pVTZ and MP2/aug-cc-pVTZ, respectively. Displacements between equilibrium geometries in the anion ground and detached states along each normal mode were estimated locally using the quadratic approximation, based on gradients calculated for the open-shell radical species, pDNB$^-$ and NO_2, at the Franck-Condon point at the MRMP2/CASSCF(15,12) and MRMP2/CASSCF(9,6) levels, respectively, using the same corresponding basis sets.

To model the angle-resolved data, the DNB anion was reoptimized using coupled cluster singles and doubles (CCSD) method, with the aug-cc-pVDZ basis set. Dyson orbitals were calculated using the equation-of-motion ionisation potential CCSD (EOM-IP-CCSD) formalism.[32,33] The Dyson orbitals were used to model the direct detachment channels for pDNB and the nitrite anion using the ezDyson program (version 3.2) developed by Krylov and co-workers.[34]

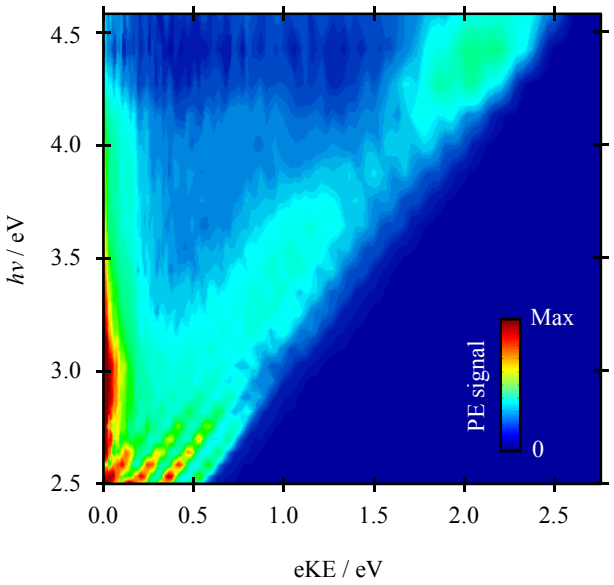

Figure 1: 2D photoelectron spectra of pDNB⁻, where each spectrum has been normalised to its integrated PE signal.

Results

The frequency-resolved PE spectra for pDNB⁻ are shown as a 2D false-colour plot in Figure 1 for the range 2.5 ≤ *hν* ≤ 4.6 eV (taken at 10 nm intervals). The PE spectra have been normalised to their total integrated intensity to emphasise spectral changes as a function of *hν*. Note that we have also taken PE spectra with *hν* < 2.5 eV (see ESI). The 2D PE spectra show a diagonal PE feature, the eKE of which increases linearly with increasing *hν*. This feature is attributed to a direct detachment channel that corresponds to an electron photodetached directly from the ground electronic state of the anion to form the ground state of the corresponding neutral species: $^2B_{2u} + h\nu \rightarrow {}^1A_g + e^-$. Figure 2 shows a representative PE spectrum at *hν* = 2.58 eV, in which the direct detachment channel is predominantly seen.

The direct detachment channel shows initial vibrational structure across the first ~0.75 eV of the continuum (see ESI). Vibrational structure comes about from the differing anion and neutral ground state geometries, leading to a Franck-Condon profile that represents this difference. A computed PE spectrum of the direct detachment channel at *hν* = 2.58 eV is also included in Figure 2, where the ion temperature is taken to be 300 K, similar to that of the experiment. The overall agreement between the measured and computed PE spectra is very good.

However, there are also clear deviations from the direct detachment peak with the PE signal at lower eKE to the diagonal feature in Figure 1. Specifically, for 2.7 < *hν* < 4.3 eV, a feature at very low eKE is visible. The appearance of very low eKE features typically indicates that a bound electronic state has been populated following internal conversion from photoexcited resonances.[11]

At *hν* ~3.0 eV the Franck-Condon profile for the direct detachment appears to change suddenly, as well as a loss of vibrational resolution, although the main vibrational progression from direct detachment can still be discerned. The PE spectra then change again around *hν* ~ 3.8 eV with more PE

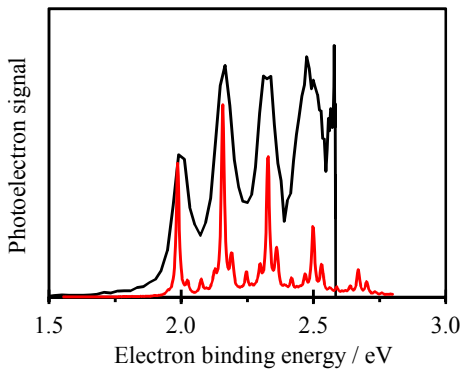

Figure 2: Measured (black) and simulated (red) photoelectron spectra (a slice of Figure 1) taken at *hν* = 2.58 eV.

signal at eKE ~ 0.6 eV. Finally, at a *hν* ~4.1 eV, a relative increase in the intensity of the direct detachment feature, as well as its broadening, is seen. For *hν* > 4.3 eV, no PE signal is seen at very low eKE.

In addition to the 2D PE, PE imaging yields PADs that give complementary information about the molecular orbital (MO) from which the electron is detached.[35,36] The PADs are fitted to the standard equation for a single photon detachment process and are quantified by the anisotropy parameters, β_2.[37] These are plotted as a 2D false-colour plot in Figure 3, where we have excluded data at eKE higher than that of the direct detachment feature, as there is no PE signal in this range and therefore no physically meaningful PADs can be extracted. β_2 parameters have limiting values of +2 and −1 for a one photon process. Figure 3 shows that the direct detachment channel has a negative β_2 value (for *hν* < 2.9 eV). Qualitatively, this is may be expected given that photodetachment is from the extended π-system of pDNB⁻, where the singly-occupied MO (SOMO) in the ground electronic state is of a π*-character.[38,39] The qualitative agreement, however, fails in regions where the 2D PE spectra

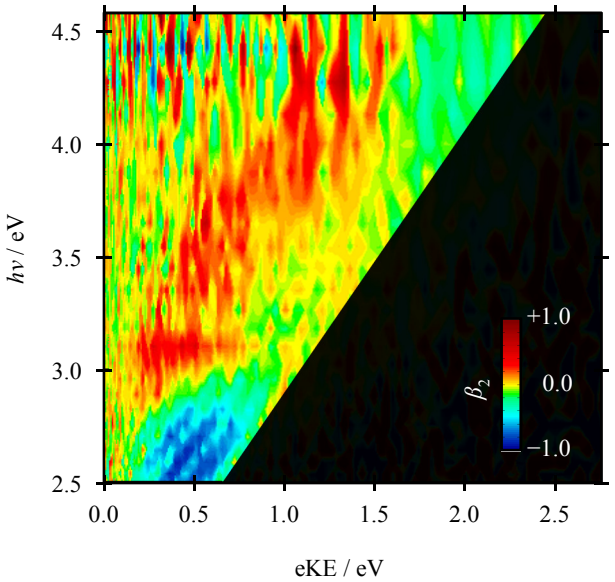

Figure 3: 2D β_2 spectra of pDNB⁻. The shaded region is ignored as there is insufficient PE signal to define a physically meaningful PAD.

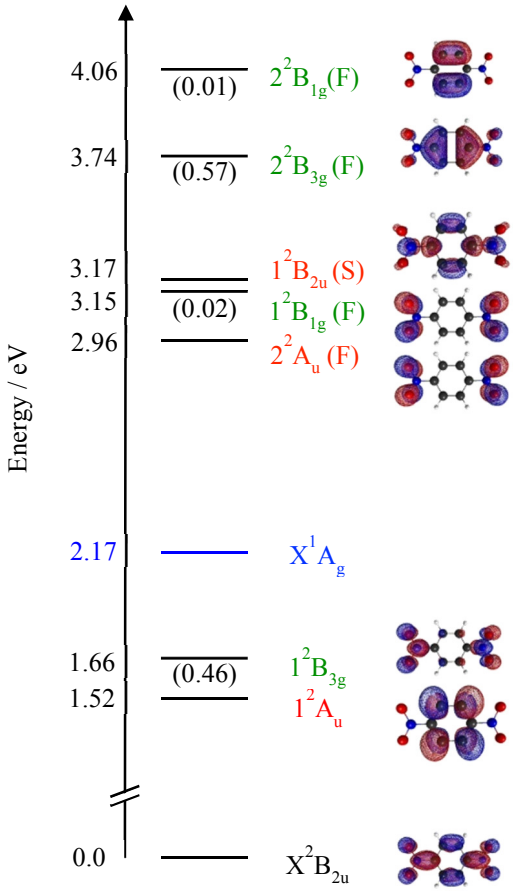

Figure 4: The calculated vertical excitation energies for $pDNB^-$ (eV). The oscillator strengths are shown in parenthesis for symmetry allowed transitions (green). The XMCQDPT2 natural orbitals that are singly occupied are shown for clarity, and the character of resonances is given alongside the symmetry label, where (F) and (S) indicate a Feshbach or shape resonance, respectively. The calculated vertical detachment energy is shown in blue. Within this energy range only the ππ* excited states are shown; the nπ* excited states, which are electronically bound and optically dark, are found to lie close to the detachment threshold at 1.90 and 1.97 eV. Note that symmetry forbidden electronic transitions (red) can gain intensity through coupling to vibrations.

show deviations from direct detachment (*i.e.* $h\nu$ > 2.9 eV). Finally, it is interesting to note that the vibrational structure of the direct detachment channel is preserved in the angle-resolved spectra as oscillations in β_2 values that match to the eKE of the vibrational bands.

The results from the electronic structure calculations are collated in Figure 4, which provide the computed transition energies and their oscillator strengths; the relevant MOs of the active space are given in the ESI.

The energy of the continuum (in the anion geometry) is calculated to lie at 2.17 eV. Figure 4 shows that there are two bound excited states, 1^2A_u and 1^2B_{3g}, which are optically dark and bright, respectively. For $h\nu$ < 4.5 eV there are additional 5 resonances. The first three resonances are clustered around 3 eV, which are the 2^2A_u, 1^2B_{1g}, and 1^2B_{2u} resonances. Only the 1^2B_{1g} state has some oscillator strength; photoexcitation to the other two resonances from the ground state is symmetry forbidden. The next 2^2B_{3g} resonance at $h\nu$ = 3.74 eV is optically bright. Finally, at $h\nu$ = 4.16 eV there is a 1^2B_{1g} resonance. All the optically active resonances are of Feshbach character in which

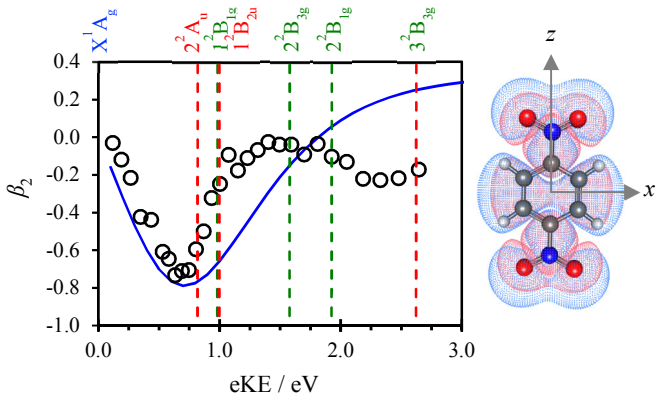

Figure 5: Measured (open circles) and computed (solid blue line) β_2 anisotropy parameters for the highest kinetic energy peak (*i.e.* the 0-0 transition). Location of resonances are shown as vertical dashed lines, including symmetry labels. The calculated β_2 parameter is derived from the Dyson orbital shown.

autodetachment must be accompanied with an electronic transition in the neutral core to reach the ^1A_g ground state of the neutral.

Finally, we have computed the β_2 values using the Dyson orbital approach for the direct detachment $^2B_{2u} + h\nu \rightarrow {}^1A_g + e^-$ channel. The results of this are shown in Figure 5. There is good agreement with the experimentally derived values at eKE less than 0.8 eV. However, coinciding with the appearance of the indirect detachment channels in Figure 1 and the computed resonance positions (also included in Figure 5), deviations are observed from the predicted behaviour, similar to our earlier observations.[35,40,41]

Discussion

Key physical properties of the pDNB can be determined from the experimental data, including the adiabatic detachment energy (ADE), vertical detachment energy (VDE), and the onset of resonances. Based on the excellent agreement between the computed and measured Franck-Condon profile of the PE spectrum in Figure 2, the 0-0 transition in Figure 1 can be identified as the peak at highest eKE (there are negligible contributions from hot-bands). From the experiment, we determine that ADE is 1.99±0.01 eV. Our value agrees with a previous PE imaging study by the Sanov group[42] and with data from ion/molecule reaction equilibria.[43,44] Our experiment also provides the VDE, which is taken as the maximum of the Franck-Condon profile of the direct detachment feature (in the absence of any resonances). We find that VDE is 2.15 eV, being in excellent agreement with the computed VDE of 2.17 eV. The dominant vibrational progression observed in the PE spectrum is due to the symmetric stretch of the two NO_2 groups. The measured vibrational spacing from Figure 2 is 163 meV which compares well with the calculated frequency of 171 meV.

In regions where spectral broadening has occurred, the apparent Franck-Condon profile is different, although the vibrational levels of the neutral can still be identified at high eKE. Deviation from direct detachment features are quite common in anion PE spectroscopy and typically come about from the excitation of an electronic resonance of the

anion.[40,45,46] Several mechanisms can lead to spectral broadening and/or red-shifting. Firstly, as the resonance has its own associated potential energy surface, the Franck-Condon factors between it and the final neutral electronic state may be different to a direct channel.[30] Secondly, as autodetachment is not instantaneous, the resonance lifetime may be sufficiently long that nuclear dynamics, including internal conversion, can take place.[47,48] Autodetachment can occur from anywhere along the trajectory of the wavepacket, up to the point where the potential energy surface of the anion becomes bound. In its extreme case, the ground state of the anion may be recovered,[48,49] and complete internal vibrational redistribution occurs. In the gas-phase, energy is conserved and so the total energy in this case remains above the ADE and electrons are lost by the statistical sampling of modes that may lead to electron emission.[50–52] Alternatively, in competition with this statistical detachment is dissociation, leading to charged fragments. For $h\nu$ > 2.5 eV, a feature that peaks at eKE ~ 0 eV is seen, thus suggesting that the ground or bound electronic states are recovered across this photon energy range.

The energetic onset of resonances can be determined in two ways: firstly, from the $h\nu$ at which an indirect signal is observed in the 2D PE spectra (Figure 1); and secondly, by sudden changes in the PADs as a function of $h\nu$, that do not follow the expected direct detachment PADs (Figure 5). Specifically, the Dyson orbital approach is unable to account for autodetachment from resonances because the model is defined by only a single initial and final state: the ground state of the anion and the neutral, respectively, for the direct detachment channel. From Figure 5, there are multiple energies at which there are deviations from the modelled PADs.

The first clear deviation from the direct detachment channel in both the PE spectra and the PADs is around $h\nu$ ~ 2.9 eV (*i.e.* eKE ~ 0.9 eV). The Franck-Condon profile changes accompanied by broadening and a loss of apparent spectral resolution. According to our calculations, there are three resonances at $h\nu$ ~ 3 eV, with the 1^2B_{1g} Feshbach resonance being the only optically bright state. The origin of the associated spectral broadening is now considered. Broadening due to rapid autodetachment can be modelled as a vertical transition (*i.e.* Franck-Condon) from resonance to the final state, as shown by Bochenkova *et al*. in the GFP chromohore.[30] The result is an indirect PE peak that does not change in eKE as $h\nu$ increases. For 2.8 < $h\nu$ < 3.8 eV, the eKE of the indirect peak is not constant with $h\nu$ and instead is increasing; it has a constant electron binding energy (eBE). We therefore consider an alternative explanation. As the initially excited resonance is of Feshbach character, the autodetachment may be expected to be relatively slow and significant nuclear dynamics can occur on the resonances. We have previously shown for radical anion quinones that internal conversion can take place prior to autodetachment and that, in the presence of a bound-electronic state, the ground electronic state can be recovered with extreme efficiency.[48] We note that $pDNB^-$ has available bound states (Figure 4) and that there is evidence of bound state recovery based on the observed statistical detachment peak near eKE = 0 eV. So how can we explain the apparent indirect PE signal that is red-shifted from the direct detachment?

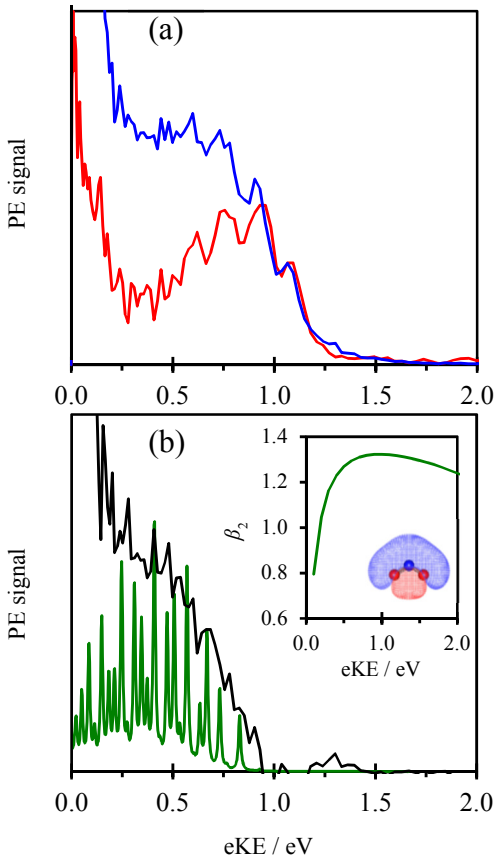

Figure 6: PE spectra taken at $h\nu$ = 3.10 eV. In (a), the PE spectra are taken using 5 ns pulses (blue) and 50 fs pulses (red). The PE spectrum in (b) is the difference between the two spectra (black) and includes a simulated PE spectrum of NO_2^- at $h\nu$ = 3.10 eV (green). Inset shows the computed β_2 anisotropy parameters expected for the lowest-energy direct photodetachment channel from the n-orbital of NO_2^-. Note that the experimental difference between the VDE and ADE values observed here at eKE of 0.4 eV and 0.8 eV, respectively, matches the calculated one.

In Figure 6(a), the PE spectra of $pDNB^-$ taken at $h\nu$ = 3.10 eV with laser pulses of ~5 ns and ~50 fs duration are shown. The high eKE edge is similar between the two spectra. However, there are clear deviations for eKE < 1 eV. There is significantly more signal at very low eKE, but both spectra suggest that statistical emission occurs and the ground (or bound) state is recovered. The most striking difference between the spectra is that the indirect peak seen at eKE ~ 0.5 eV in the ns spectrum is not present in the fs spectrum. If this indirect feature arises from autodetachment of the initially populated resonances, then the duration of the excitation field should have no effect. Hence, the origin of the indirect process appears not to be autodetachment from resonances. Figure 6(b) shows a difference spectrum between the 5 ns and 50 fs spectra, which recovers the spectral shape of the indirect peak. The VDE of the difference spectrum is at ~2.7 eV and the ADE at ~2.3 eV and has a striking resemblance to the PE spectrum of NO_2^- taken by Ervin *et al.*, which has a broad peak with VDE = 2.7 eV and ADE = 2.273±0.005 eV.[53] In Figure 6(b), we include a simulation of

the expected PE spectrum at $h\nu$ = 3.10 eV of NO_2^-, shifted so that the 0-0 transition lines up with the known ADE. Our

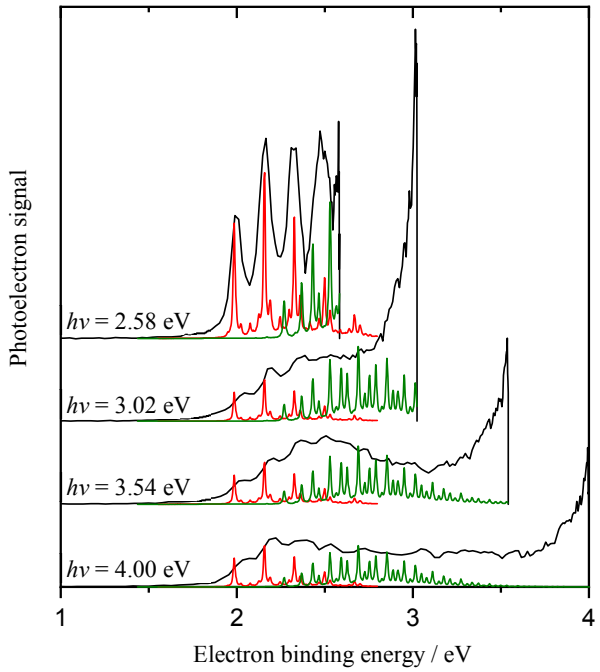

Figure 7: Slices of PE spectra (black) that are representative of regions where resonances play an important role as seen in Figure 1. The PE spectra have been offset with respect to one another to aid clarity in comparison. Included for each photon energy are the simulated direct PE spectrum for $pDNB^-$ (red) and NO_2^- (green).

simulated spectrum closely resembles that of Ervin *et al.* and shows good agreement with the difference PE spectrum shown in Figure 6(b). We do not have the resolution to observe the dense vibrational structure.

The NO_2^- PE spectrum can be generated by the absorption of a second photon during the 5 ns pulse. The dissociation is most likely a ground state or bound excited states process because there is clear evidence that the bound electronic states are recovered. Hence, NO_2^- loss is a relatively slow process and does not occur during the 50 fs pulse and can therefore not be seen in the PE spectrum using pulses shorter than the dissociation timescale. Similar dynamics have been observed following photoexcitation in anions that then undergo ground state reactions.[54]

The NO_2^- PE spectrum can in fact explain much of the spectral broadening observed in Figure 1. In Figure 7, representative 1D PE spectra are shown along with simulated PE spectra for direct detachment from $pDNB^-$ and NO_2^-. The simulated PE spectra have been arbitrarily scaled to the experimental data. The high eKE edge is consistent with direct detachment. The NO_2^- spectrum on the other hand is very broad, leading to the broad unresolved peak in Figure 7, that remains constant in eBE (and shifts linearly with eKE – see Figure 1). At CAM-B3LYP/aug-cc-pVDZ the binding energy of NO_2^- is 2.59 eV, which is consistent with the energy range, where the NO_2^- formation is observed.

The PADs support the above interpretation. For $h\nu$ > 2.9 eV, the β_2 anisotropy parameter is more positive (β_2 ~ +0.5) to the low eKE edge of the direct detachment peak. This low eKE edge corresponds to the signal that we assigned to the NO_2^- PE spectrum. As the photodetachment of NO_2^- and $pDNB^-$ are incoherent, we expect to predominantly observe the PAD expected for NO_2^- at the eKE where this feature dominates. We have computed the PADs for photodetachment from NO_2^- and the expected β_2 as a function of eKE for this channel is inset in Figure 6(b). The detachment is very anisotropic with β_2 > 0 across the range probed here. This is consistent with the observed β_2 ~ +0.5 for the feature we assigned to NO_2^- photodetachment. The quantitative discrepancy is likely a consequence of the fact that other PE signals contribute over this energy range such as the high eKE channel and the very low eKE peak – both of which are predominantly isotropic (see Figure 3) and thus reduce the observed β_2 from NO_2^- photodetachment. The isotropic nature of the direct detachment comes about because of the influence of the resonances that are excited (see Figure 5).

From Figure 1 and 7, the NO_2^- photodetachment feature is apparent up to $h\nu$ ~ 4.1 eV. However, between 3.8 < $h\nu$ < 4.1 eV, additional PE signal can be seen essentially at all eKE between the direct detachment feature and the feature near 0 eV. Our calculations show that the 2^2B_{3g} resonance lies at 3.74 eV and is optically brighter than other resonances. The PE spectrum at $h\nu$ = 4.00 eV (Figure 7) shows that even more spectral broadening has occurred beyond that predicted by the PE spectrum of NO_2^-. The 2^2B_{3g} resonance is of Feshbach character and autodetachment may occur along various parts of the potential energy surface. Note also that the peak at very low eKE is smaller here suggesting that more autodetachment has occurred (leading to less ground/bound electronic state recovery).

Finally, for $h\nu$ > 4.1 eV, there is again a change in the PE spectra. The spectra are dominated by a single peak at high eKE and the statistical electron loss channel becomes a very minor component. The peak at high eKE is broadened relative to a simple direct detachment process. Hence, a new excitation channel appears to be accessed here. Our calculations show that the 2^2B_{1g} resonance lies at this energy and can account for the observed change. Note that β_2 for the high eKE peak is slightly negative (~–0.2), while the predicted β_2 based on direct detachment is positive (~+0.2), again consistent with the excitation of a resonance (see Figure 5).

Overall, the observed resonance dynamics in $pDNB^-$ have many similarities with electron impact studies on pDNB. Specifically, these show that NO_2^- is a major dissociative electron attachment channel from ~ 1 eV above threshold (below 1 eV, no NO_2^- was observed). This corresponds to $h\nu$ ~ 3 eV in the 2D PE spectra, above which, indeed, the spectral feature corresponding to NO_2^- photodetachment is clearly observed. Sulzer *et al*. have shown that the yield of NO_2^- is essentially constant between electron energies of 1.3 and 2.5 eV, above which it rises sharply.[23] In the 2D PE spectra, this energy corresponds to $h\nu$ > 4.5 eV. At this energy, we still observe the NO_2^- photodetachment feature, but also observe another indirect (autodetachment) channel. However, there are also key differences between the PE spectroscopy and electron attachment. Specifically, the latter only shows parent

anion formation over the electron energies near threshold (up to 0.2 eV). In contrast, we observe ground state recovery up to *hv* ~ 4.3 eV (corresponding to electron energies of 2.2 eV). Additionally, the electron impact studies showed many dissociative electron attachment channels.[23,24] These are not observed here, but that does not mean that they are not active and we may simply be blind to other charged products in the experiment because of small photodetachment cross sections, too high electron affinities, or because the timescale for their formation is beyond that probed here (~5 ns). Note also that Rydberg electron transfer experiments point to the existence of a quadrupole-bound non-valence state in $pDNB^-$.[55] Here, we see no evidence for this in the PE spectra, although PE spectroscopy in general can be quite sensitive to such non-valence states.

Conclusion

The high density of resonances in $pDNB^-$ has been probed experimentally and modelled computationally. The electron affinity of pDNB is determined to be 1.99±0.01 eV. The 2D photoelectron spectra as well as angular distributions show the presence of several resonances. Good overall agreement is achieved between experimental and theory. Bound electronic states recovery is inferred from the observation of statistical electron loss. Comparison between photoelectron spectra taken with our ns and fs excitation source allows us to identify a dissociative channel that leads to formation of the NO_2^- photofragment.

This study illustrates the breadth of processes than can be probed using 2D photoelectron imaging and highlights the necessity for computational models being able to disentangle the rich signatures observed. Vertical excitation energies and photoelectron spectra of $pDNB^-$ are calculated at the XMCQDPT2 level and angular distributions for direct electron detachment is modelled using the Dyson orbital approach. These provide qualitative and quantitative agreement with our experimental results. Through development of this joint computational and experimental approach to probing the electronic structure of anions in the gas phase, we will now be able to explore a wide range of intervalence charge transfer systems and elucidate their intrinsic properties with confidence.

Conflicts of interest

There are no conflicts to declare.

Acknowledgements

The experimental part of this work has been supported by the European Research Council (Starting Grant 306536). C.S.A. and A.V.B. acknowledge support from the Russian Foundation for Basic Research (Grant no. 17-33-50191). The research is carried out using the equipment of the shared research facilities of HPC computing resources at Lomonosov Moscow State University. Work has been partly conducted using the resources of the iOpenShell Centre for Computational Studies of Electronic Structure and Spectroscopy of Open-Shell and Electronically Excited Species (http://iopenshell.usc.edu).

References

1 I. Shimamura and K. Takayanagi, *Electron-Molecule Collisions*, Springer US, Boston, MA, 1985.
2 L. G. Christophorou and J. K. Olthoff, *Fundamental Electron Interactions with Plasma Processing Gases*, Springer US, Boston, MA, 2004.
3 G. J. Schulz, *Rev. Mod. Phys.*, 1973, **45**, 378–422.
4 H. Hotop, M.-W. Ruf, M. Allan and I. I. Fabrikant, in *Advances in Atomic Molecular and Optical Physics*, 2003, vol. 110, pp. 85–216.
5 K. D. Jordan and P. D. Burrow, *Chem. Rev.*, 1987, **87**, 557–588.
6 T. Reddish, F. Currell and J. Comer, *J. Phys. E. Sci. Instrum.*, 1988, **36**, 203–207.
7 F. Currell and J. Comer, *Phys. Rev. Lett.*, 1995, **74**, 1319–1323.
8 K. Regeta and M. Allan, *Phys. Rev. Lett.*, 2013, **110**, 203201.
9 M. Allan, K. Regeta, J. D. Gorfinkiel, Z. Mašín, S. Grimme and C. Bannwarth, *Eur. Phys. J. D*, 2016, **70**, 123.
10 J. R. R. Verlet, D. A. Horke and A. S. Chatterley, *Phys. Chem. Chem. Phys.*, 2014, **16**, 15043.
11 C. S. Anstöter, J. N. Bull and J. R. R. Verlet, *Int. Rev. Phys. Chem.*, 2016, **35**, 509–538.
12 J. P. Rogers, C. S. Anstöter and J. R. R. Verlet, *J. Phys. Chem. Lett.*, 2018, **9**, 2504–2509.
13 M. B. Robin and P. Day, in *Advances in Inorganic Chemistry and Radiochemistry*, Academic Press, Waltham, MA, 1967, p. 247–422.
14 A. Heckmann and C. Lambert, *Angew. Chemie Int. Ed.*, 2012, **51**, 326–392.
15 J. Hankache and O. S. Wenger, *Chem. Rev.*, 2011, **111**, 5138–5178.
16 A. J. Cohen, P. Mori-Sánchez and W. Yang, *Chem. Rev.*, 2012, **112**, 289–320.
17 P. Mori-Sánchez, A. J. Cohen and W. Yang, *Phys. Rev. Lett.*, 2008, **100**, 146401.
18 C. Sutton, T. Körzdörfer, V. Coropceanu and J.-L. Brédas, *J. Phys. Chem. C*, 2014, **118**, 3925–3934.
19 A. A. Granovsky, *J. Chem. Phys.*, 2011, **134**, 214113.
20 S. F. Nelsen, M. N. Weaver, A. E. Konradsson, J. P. Telo and T. Clark, *J. Am. Chem. Soc.*, 2004, **126**, 15431–15438.
21 T. B. Brill and K. J. James, *Chem. Rev.*, 1993, **93**, 2667–2692.
22 E. de Hoffmann and V. Stroobant, *Mass Spectrometry - Principles and Applications.*, John Wiley & Sons, Chichester, Second Edi., 2007.
23 P. Sulzer, A. Mauracher, S. Denifl, M. Probst, T. D. Märk, P. Scheier and E. Illenberger, *Int. J. Mass Spectrom.*, 2007, **266**, 138–148.
24 A. Mauracher, S. Denifl, A. Edtbauer, M. Hager, M. Probst, O. Echt, T. D. Märk, P. Scheier, T. A. Field and K. Graupner, *J. Chem. Phys.*, 2010, **133**, 244302.
25 J. Lecointre, G. M. Roberts, D. A. Horke and J. R. R. Verlet, *J. Phys. Chem. A*, 2010, **114**, 11216–24.

26 L. H. Stanley, C. S. Anstöter and J. R. R. Verlet, *Chem. Sci.*, 2017, **8**, 3054–3061.

27 G. M. Roberts, J. L. Nixon, J. Lecointre, E. Wrede and J. R. R. Verlet, *Rev. Sci. Instrum.*, 2009, **80**, 053104.

28 Y. Shao, Z. Gan, E. Epifanovsky, A. T. B. Gilbert, M. Wormit, J. Kussmann, A. W. Lange, A. Behn, J. Deng, X. Feng, D. Ghosh, M. Goldey, P. R. Horn, L. D. Jacobson, I. Kaliman, R. Z. Khaliullin, T. Kuś, A. Landau, J. Liu, E. I. Proynov, Y. M. Rhee, R. M. Richard, M. A. Rohrdanz, R. P. Steele, E. J. Sundstrom, H. L. Woodcock, P. M. Zimmerman, D. Zuev, B. Albrecht, E. Alguire, B. Austin, G. J. O. Beran, Y. A. Bernard, E. Berquist, K. Brandhorst, K. B. Bravaya, S. T. Brown, D. Casanova, C.-M. Chang, Y. Chen, S. H. Chien, K. D. Closser, D. L. Crittenden, M. Diedenhofen, R. A. DiStasio, H. Do, A. D. Dutoi, R. G. Edgar, S. Fatehi, L. Fusti-Molnar, A. Ghysels, A. Golubeva-Zadorozhnaya, J. Gomes, M. W. D. Hanson-Heine, P. H. P. Harbach, A. W. Hauser, E. G. Hohenstein, Z. C. Holden, T.-C. Jagau, H. Ji, B. Kaduk, K. Khistyaev, J. Kim, J. Kim, R. A. King, P. Klunzinger, D. Kosenkov, T. Kowalczyk, C. M. Krauter, K. U. Lao, A. D. Laurent, K. V Lawler, S. V Levchenko, C. Y. Lin, F. Liu, E. Livshits, R. C. Lochan, A. Luenser, P. Manohar, S. F. Manzer, S.-P. Mao, N. Mardirossian, A. V Marenich, S. A. Maurer, N. J. Mayhall, E. Neuscamman, C. M. Oana, R. Olivares-Amaya, D. P. O'Neill, J. A. Parkhill, T. M. Perrine, R. Peverati, A. Prociuk, D. R. Rehn, E. Rosta, N. J. Russ, S. M. Sharada, S. Sharma, D. W. Small, A. Sodt, T. Stein, D. Stück, Y.-C. Su, A. J. W. Thom, T. Tsuchimochi, V. Vanovschi, L. Vogt, O. Vydrov, T. Wang, M. A. Watson, J. Wenzel, A. White, C. F. Williams, J. Yang, S. Yeganeh, S. R. Yost, Z.-Q. You, I. Y. Zhang, X. Zhang, Y. Zhao, B. R. Brooks, G. K. L. Chan, D. M. Chipman, C. J. Cramer, W. A. Goddard, M. S. Gordon, W. J. Hehre, A. Klamt, H. F. Schaefer, M. W. Schmidt, C. D. Sherrill, D. G. Truhlar, A. Warshel, X. Xu, A. Aspuru-Guzik, R. Baer, A. T. Bell, N. A. Besley, J.-D. Chai, A. Dreuw, B. D. Dunietz, T. R. Furlani, S. R. Gwaltney, C.-P. Hsu, Y. Jung, J. Kong, D. S. Lambrecht, W. Liang, C. Ochsenfeld, V. A. Rassolov, L. V Slipchenko, J. E. Subotnik, T. Van Voorhis, J. M. Herbert, A. I. Krylov, P. M. W. Gill and M. Head-Gordon, *Mol. Phys.*, 2015, **113**, 184–215.

29 A. A. Granovsky, Firefly, version 8.2.1, http://classic.chem.msu.su/gran/firefly/index.html.

30 A. V. Bochenkova, C. R. S. Mooney, M. A. Parkes, J. L. Woodhouse, L. Zhang, R. Lewin, J. M. Ward, H. C. Hailes, L. H. Andersen and H. H. Fielding, *Chem. Sci.*, 2017, **8**, 3154–3163.

31 A. V. Bochenkova, B. Klaerke, D. B. Rahbek, J. Rajput, Y. Toker and L. H. Andersen, *Angew. Chemie Int. Ed.*, 2014, **53**, 9797–9801.

32 C. M. Oana and A. I. Krylov, *J. Chem. Phys.*, 2009, **131**, 124114.

33 C. Melania Oana and A. I. Krylov, *J. Chem. Phys.*, 2007, **127**, 234106.

34 S. Gozem and A. I. Krylov, ezDyson, http://iopenshell.usc.edu/downloads/ezdyson.

35 C. W. West, J. N. Bull, E. Antonkov and J. R. R. Verlet, *J. Phys. Chem. A*, 2014, **118**, 11346–11354.

36 C. S. Anstöter, C. R. Dean and J. R. R. Verlet, *J. Phys. Chem. Lett.*, 2017, **8**, 2268–2273.

37 J. Cooper and R. N. Zare, *J. Chem. Phys.*, 1968, **48**, 942–943.

38 A. Sanov, *Annu. Rev. Phys. Chem.*, 2014, **65**, 341–363.

39 E. R. Grumbling and A. Sanov, *J. Chem. Phys.*, 2011, **135**, 164302.

40 C. S. Anstöter, C. R. Dean and J. R. R. Verlet, *Phys. Chem. Chem. Phys.*, 2017, **19**, 29772–29779.

41 C. W. West, J. N. Bull, A. S. Hudson, S. L. Cobb and J. R. R. Verlet, *J. Phys. Chem. B*, 2015, **119**, 3982–3987.

42 K. Pichugin, University of Arizona, 2010.

43 S. Chowdhury, E. P. Grimsrud, T. Heinis and P. Kebarle, *J. Am. Chem. Soc.*, 1986, **108**, 3630–3635.

44 E. K. Fukuda and R. T. McIver, *J. Am. Chem. Soc.*, 1985, **107**, 2291–2296.

45 J. L. Woodhouse, M. Assmann, M. A. Parkes, H. Grounds, S. J. Pacman, J. C. Anderson, G. A. Worth and H. H. Fielding, *Phys. Chem. Chem. Phys.*, 2017, **19**, 22711–22720.

46 R. F. Gunion, M. K. Gilles, M. L. Polak and W. C. Lineberger, *Int. J. Mass Spectrom. Ion Process.*, 1992, **117**, 601–620.

47 D. A. Horke, Q. Li, L. Blancafort and J. R. R. Verlet, *Nat. Chem.*, 2013, **5**, 711–717.

48 J. N. Bull, C. W. West and J. R. R. Verlet, *Chem. Sci.*, 2015, **6**, 1578–1589.

49 J. N. Bull, C. W. West and J. R. R. Verlet, *Phys. Chem. Chem. Phys.*, 2015, **17**, 16125–35.

50 O. W. Richardson, *Proc. Cambridge Philos. Soc.*, 1901, **11**, 286.

51 A. Amrein, R. Simpson and P. Hackett, *J. Chem. Phys.*, 1991, **95**, 1781–1800.

52 E. E. B. Campbell, G. Ulmer and I. V. Hertel, *Phys. Rev. Lett.*, 1991, **67**, 1986–1988.

53 K. M. Ervin, J. Ho and W. C. Lineberger, *J. Phys. Chem.*, 1988, **92**, 5405–5412.

54 C. W. West, J. N. Bull and J. R. R. Verlet, *J. Phys. Chem. Lett.*, 2016, **7**, 4635–4640.

55 C. Desfrançois, V. Périquet, S. A. Lyapustina, T. P. Lippa, D. W. Robinson, K. H. Bowen, H. Nonaka and R. N. Compton, *J. Chem. Phys.*, 1999, **111**, 4569.